Volume 14, Issue 3, 152429 (1-13)

Iranian Journal of Catalysis (IJC)

https://doi.org/10.57647/j.ijc.2024.1403.29

Eco-friendly synthesis of Fe_3O_4 and its surface fabrication: Application in dye removal- a comparative study

Raju Shekhanavar, Santosh Khatavi, Kantharaju Kamanna*

Department of Chemistry, Rani Channamma University, Belagavi, Karnataka, India.

***Corresponding author:** kk@rcub.ac.in

Original Research

Received:
21 March 2024
Revised:
23 May 2024
Accepted:
7 July 2024
Published online:
10 July 2024

Abstract:

The present work describes comparative studies of Methylene blue, Methyl orange, and Calcon-carboxylic acid (MB, MO, and CCA) dyes adsorption in the presence of sunlight using novel sulfonic acid-carbon fabricated iron oxide. The preparation and characterization of the catalysts performed FT-IR, FE-SEM, EDX, VSM, & TG-DTA and reported in the previous paperwork. In this paper, the photocatalytic properties of the prepared catalyst and its intermediate materials were evaluated in the presence of sunlight to remove the dye MO, MB, and CCA. The comparative studies revealed that, the functionalized catalysts (Fe_3O_4@C-SO_3H) excelled better photocatalysis (optimized quantity 30 mg) performance in the sunlight and MWI. The adsorption reaction was monitored by a UV-Vis spectrophotometer with λ_{max} of 664 nm for MB, 590 nm for MO, and 550 nm for CCA. The dye removal in the solution was observed at 95.98% for MB, 82.55% for MO, and 83.7% for CCA in the presence of sunlight. It's worth to mention that, the novel photocatalyst core iron oxide prepared by agro-waste extract under dual function concept, where extracted medium used for the preparation of the core shell Fe_3O_4, and its biochar residue employed for the carbonization. Hence, the method developed more on green chemistry protocol, and the inexpensive catalyst used for dye adsorption phenomenon dominates than the dye degradation.

Keywords: Agro-waste; Eco-friendly; Magnetic; Photo catalytic; Surface functionalization

1. Introduction

Environmental pollution, especially water contamination, is one of the major problems, and it is serious concern as they interfere with public health and environmental quality [1–5]. The wide range of chemical discharges from pharmaceuticals [6], disinfection [7], and by-products from various industries (paper, dyes, cosmetic, food, etc.) leads pollution[8]. One of the research areas was influenced enormously in the natural remediation of water [9, 10], due to its universal solvent nature, and achieving quality of water in the present days are challenging [11, 12]. The Lack of fresh-water resources occurs due to the huge discharge of pollutants into the water bodies, which has made it challenging for the treatment in the last decade [13, 14]. Among the effluents, one of the major contributions of organic pollutants are dye [15], which is derived from synthetic with complex structures [16]. The organic dyes broadly classified into cationic, anionic, and non-ionic, azo dyes containing azo groups (-N=N-) have emerged as a special class of the synthetic dyes that are extensively used in the textile industries. These dyes are usually carcinogenic and toxic, directly affecting the aquatic ecosystem, photosynthesis, and stopping aquatic growth, and also disruption of the reproductive process, causing health issues [17, 18]. Literature reported that up to 20% of the dyes used in textile industries are dumped into the environment, producing mutagenicity into aquatic life and human health [19]. Methylene blue (MB) is a cationic dye derived from the phenothiazines tricyclic family, employed as a drug molecule, and extensively used in the textile industries as a blue colorant. But more exposure to the MB is also dangerous to aquatic life and human,

due to skin allergic, and cardiovascular and sensory organs [20]. MO (Methyl orange) is an anionic azo dye; it is also dangerous to aquatic life and the environment. Hence it must be treated before being discharged into the environment [21]. MO is resistant to degradation and soluble in water; take it out from aqueous medium is a difficult task employing present water treatment techniques. But if not properly treated, these dyes before entering into the freshwater system, cause severe aquatic and environment living beings [22]. CCA is a naphthylazo dye used as an indicator for complexometric titrations. It behaves as an anionic dye, and soluble in ethanol or basic conditions.

The major contribution of water pollution is caused by untreated dye waste produced from various industrial activities. The Present scenario has an urgent requirement of sustainable technology for the treatment of dye effluent to safeguard water [23]. Thus, in the literature reported various techniques for the treatment of wastewater to minimize public health and environmental issues. There is a wide range of techniques reported, including electrochemical and photocatalytic combined treatments, sonochemical, photo-catalytic degradation, electrochemical, biodegradation, nano-filtration, adsorption process, oxidation, chemical coagulation or flocculation, chemical precipitation, ozonation, reverse osmosis, cloud point extraction, ion-exchange, and ultra-filtration [24]. The Adsorption method differs from other techniques, gave efficiently remove the colorant from the concentrated effluent. To remove contaminants from the complicated waste, adsorption is the utmost preferred and efficient approach emerged for water pollution treatment [25]. Several research groups discovered efficient noble adsorbents, such as zeolites [26], activated carbon [27], chitosan [28], clay minerals [29], and functionalized polymers [30], etc., have improved steadily over the last decade. This is because the cost-effectiveness and quality of the adsorbent are directly involved in the efficient separation. Unfortunately, many of these adsorbents showed demerits of expensive and inefficiency. Recently, researchers reported nano–adsorbents derived from agro-waste are inexpensive such as *citrus limon* wood waste [31], orange-peel powder [32], and litchi peel [33] are emerged as a very good adsorption properties for the removal of metal ions. The solid-liquid separation of often related with only NPs was avoided by such advanced type of adsorbent–magnetic nano adsorbent with the help of an external magnetic field. High adsorption could be achieved for the new adsorbent because of increased surface-to-volume ratio with other physicochemical properties such as easy synthesis, recycle and modified through coating and functionalization, inexpensive, eco-friendliness, and lack of secondary pollutants. Recently reported dyes removal from the waste water using activated carbon of walnut shell [34], and its MNPs loaded [35].

In the literature, the well-reported efficiency of the dye degradation processes can be speed-up by using photocatalysis, it is a semiconductor material enable to absorbing light photon and accelerating reaction [36]. Among various materials discovered, Fe_3O_4 is one of the emerging photocatalysts used in the photocatalytic dye degradation application [37]. Because of its inexpensive synthesis, no secondary pollutants production, n-type semi-conducting having a band gap of E_g=2.1 eV [38]. Further, Fe_3O_4 and its composite materials are potentially demonstrated in various fields and processes such as sensors, biomedical, adsorption, super capacitor, Li-ion batteries, solar cells, hydrogen production, and dye degradation as a photocatalyst [39–43]. In the last few decades, MNPs have been attracted to a greater extent by the researchers, due to their additional magnetic attraction, enables easy separation in the reaction as an external magnet [44]. Various synthetic routes have been reported for the preparations of MNPs in the literature, are solvothermal, hydrothermal, co-precipitation, and electrothermal methods [45]. These methods employed chemicals, surfactants and reducing agents [46, 47]. Many of the preparation methods employed hazardous chemicals, which are of concern to the environment [48]. Hence, in recent years, researchers are exploring alternative synthetic routes, which are inexpensive, non-toxic, and eco-friendly [49]. Fe_3O_4 possesses a wide range of surface functionalities, and it has shown numerous applications in both synthesis and dye degradation studies (Table 1). The functionalized iron oxide NPs are a kind of material achieved by the coating on the surface of the iron oxide. Especially the adsorption of the dye takes place on the surface of the heterogeneous catalyst due to the interaction between the dye and the catalyst surface, this will happen because of the various interactions, either electrostatic and/or Vander Waals [50, 51]. Another important aspect is the negative enthalpy, and loss of entropy also leads to the dye to adsorb on the surface of the catalyst [52]. The controlling mechanism of the adsorption phenomenon is a chemical reaction, diffusion control, or the mass transfer coefficient technique is employed to determine the kinetic models [53]. The type of kinetics adsorption on the adsorbent material is decided on the operating conditions of full-scale batch process [54].

In this work, agro-waste lemon peel ash extract medium was employed for the synthesis of Fe_3O_4 NPs, and bio-char left over after the filtration was employed for the functionalization through the hydrothermal method, thereby achieving "one source with two functions." The resultant Fe_3O_4 NPs was functionalized by carbonization and sulfonation gave magnetic carbon-based solid acid (Fe_3O_4@C-SO_3H). The method employed eco-friendly, inexpensive, and non-toxic alternative methods achieved magnetic NPs. The physicochemical properties of the prepared MNPs were characterized using various techniques. The comparative studies were performed using Fe_3O_4, Fe_3O_4@C, and Fe_3O_4@C-SO_3H for the dye degradation of MB, MO, and CCA. The mesoporous carbon largely covering the surface of the Fe_3O_4 core, not only stabilizes the Fe_3O_4 MNPs against aggregation and oxidation of the Fe_3O_4 MNPs, but also coordinates grafting with SO_3H groups as a Bronsted acid for many practical applications. The dye removal studies revealed that, the catalyst was a more active site to adsorb MB and decolourized at a faster rate of 95.63%, 82.55% for MO, and 88.53% for CCA. Further, a faster rate of adsorption of the dye compared to sun-light was noticed with the microwave irradiation method. To enhance the adsorption

Table 1. A List of Fe_3O_4 based composite material prepared and used for the dye degradation.

Fe_3O_4 functionalised	**Dye**	**Medium/condition**	**% of degradation [Ref]**
Fe_3O_4(Pd/HAP/ Fe_3O_4)	MR	H_2O_2/rt	58.0 [55]
	MO		63.2 [55]
	MY		65.2 [55]
Porous Fe_3O_4 NPs/PVP	Xylenol orange	H_2O_2/US	94.0 [56]
Fe_3O_4/SiO_2-Pr-s-Ag	4-nitrophenol	$NaBH_4$/rt	80.0 [57]
	MB		75.0 [57]
Fe_3O_4@Nb@Mo	MB	H_2O_2/UV/US	75.0 [57]
	MO		60.0 [58]
Fe_3O_4 NPs	Reactive orange 107	H_2O_2/US	93.3 [59]
Fe_3O_4@ZnO	MO	H_2O_2/US	94.0 [60]
	Eriochromsch warz T		57.0 [60]
	Eosin T		42.0 [60]
	RB		34.0 [60]
Fe_3O_4@Mn_3O_4	MB	Mangane/rt	93.0 [61]
Fe_3O_4@Ni NPs	Congo red	H_2O/UV	79.0 [61]
	MB		89.0 [62]
	RB		81.0 [62]
Fe_3O_4@n-NH_2	MB	$NaBH_4$/rt	80.0 [63]
	MO		79.0 [63]
Fe_3O_4@n-NH_2	MB	H_2O/UV	91.9 [63]
	MO		82.5 [63]
Fe_3O_4@TiO_2	MB	H_2O/UV	92.3 [64]
	MO		82.5 [64]
Fe_3O_4@C-SO_3H	**MB**	**Sun light/MWI [present work]**	**95.9**
	MO		**82.5**
	CA		**83.7**

phenomenon, an equilibrium isotherm, thermodynamics kinetics adsorption study of MB as Fe_3O_4@C-SO_3H and other precursors MNPs were established.

2. Experimental

2.1 Preparation of lemon peel water extract

Fresh lemon is collected from the local and is peeled. The peels were washed with tap water then by distilled water to remove the dirt particles, and then dried on open sunlight and burnt on a Bunsen burner to get lemon peel ash. The obtained 10 g of finely powdered ash was soaked in 100 mL of dd (double distilled) water, suspended, and stirred at rt for 1 h. The suspension was dark brown in colour, then the suspension was filtered to get a Water Extract of Lemon Fruit Shell Ash (WELFSA), and it was directly used for the preparation of iron oxide NPs [65].

2.2 Preparation of Fe_3O_4 using WELFSA

3.0 g of $FeSO_4.7H_2O$ and 3.2 g of $FeCl_3.6H_2O$ were weighed separately and taken in a 250 mL beaker, added 50 mL of dd water. To this reaction, a mixture added 10 mL of WELFSA, then stirred for about 45 min at 90 °C for about 45 min, added cooled to attain it then basified with the addition of NH_4OH solution dropwise till black precipitate formation stopped, and then allowed to settle down. The black precipitate formed was held by an external magnet, and washed several times with dd water followed by ethanol. The obtained residue was calcinated in a muffle furnace at 700 °C for about 5 h, and stored in an air-tight container for further use.

2.3 Synthesis of Fe_3O_4@C

The bio-char residue after the filtration presents from the lemon peel ash extract taken 10 g in a 500 mL beaker, and added 100 mL of dd water, and continued stirring at rt for 1h. Added 3 g of the above prepared Fe_3O_4 NPs, and the resultant solution was dispersed in an ultrasonic bath for about 30 min. Then the whole solution was transferred to a 100 mL Teflon-lined stainless-steel autoclave, and kept at 180 °C in an oven for 10 h. The carbonized material is magnetically attracted washed with water and ethanol thoroughly, and dried at 70 °C in an oven under vacuum for 10 h gave powder product denoted as Fe_3O_4@C.

2.4 Synthesis of Fe_3O_4@C-SO_3H

Above prepared Fe_3O_4@C (1.5 g) weighed in a 50 mL beaker, and 10 mL of Con. H_2SO_4 was added to this and stirred at rt. After 45 min of stirring, the solution was transferred into a Teflon-lined autoclave and kept at 160 °C in an oven for about 12 h. After cooling to rt, the black solid held by an external magnet, washed with hot dd water, and ethanol for 2-3 times, dried at 60 °C in an oven under vacuum for 12 h, and denoted as Fe_3O_4@C-SO_3H.

2.5 Solid acid titration

The iron oxide functionalized sulfonic acid was titrated by acid-base reaction method. Briefly, 25 mg of the catalyst was taken in a 50 mL of (0.01 M) NaOH solution in a 100 ml conical flask, this reaction mixture was kept at rt for

about 2 h. Then, the catalyst was filtered by using the strong magnet and washed with dd water (5 mL) for about two times. After that, the filtrate was titrated to neutrality using a 0.01 M HCl using phenolphthalein as an indicator. The total acid group on Fe_3O_4@C-SO_3H MNPs was found to be 0.47 mmol/g.

2.6 Reduction of 4-nitrophenol

The prepared catalysts (Fe_3O_4@C-SO_3H) reduction properties is examined in the presence of sodium borohydride and 4-nitrophenol (4-NP) at rt. Typically taken 2 mL of aqueous 4-NPs (0.15 mM) and 100 μL of aq. $NaBH_4$ (50 mM) in a 4 mL quartz cuvette, and added 1 mg of Fe_3O_4@C-SO_3H. The cuvette was placed in a UV-Vis spectrophotometer, and the progress of the reaction was monitored at different time intervals.

2.7 Reduction of methylene blue dye

Fe_3O_4@C-SO_3H NPs in the presence of $NaBH_4$ was used to study the reduction of MB dye at rt (28-30 °C). Briefly, in a 4 mL quartz cuvette, aqueous solution of 2 mL MB (10 ppm) and 100 μL of $NaBH_4$ (30 mM) were placed and 1 mg of catalysts added. The cuvette was placed in a UV-Visible spectrophotometer and progress of the reaction was monitored at different time intervals.

2.8 Materials

Chemicals were purchased from Avra and sd-fine and were directly used without purification. The lemon fruit *(Citrus limon)* peel was collected from Belagavi, Karnataka, India. The XRD data was recorded using PAN analytical (X-pert PRO). The surface morphology and elemental mapping were analysed using EDS by TESCAN and Bruker [(MIRA 3 (FESEM) and Quantax 200 (EDS), Evactron XEI (plasma cleaner)]. TG-DTA was recorded by NETZSCH (STA 2000). The magnetic properties were determined by a Vibrating Sample Magnetometer (VSM).

3. Result and discussion

In this work reported greener protocol synthesis of Fe_3O_4 NPs starting with $FeCl_3$ and $FeSO_4$ in the presence of agro-waste Water Extract of Lemon Fruit Shell Ash (WELFSA) as a catalytic solvent medium. The method developed showed inexpensive and chemical-free synthesis gave free-flowing Fe_3O_4 MNPs. Further, the mesoporous carbon is fabricated on the surface of iron oxide, where it is stabilized Fe_3O_4 against aggregation and also prevents oxidation and extended to coordinated or grafted with SO_3H as a Bronsted acid. Lemon peel ash biomass waste was used as a carbon source for the synthesis of the novel magnetic carbon-based solid acid by a hydrothermal method. To increase the acidity of the catalyst, the sulfonation was done by sulfuric acid at 180 °C in a sealed Teflon-lined autoclave gave Fe_3O_4@C-SO_3H (Fig. 1). The obtained magnetic catalyst Fe_3O_4@C-SO_3H was characterized by various spectroscopic and microscopic techniques such as SEM-EDX, XRD, FT-IR, VSM, TGA and XRF. (Manuscript submitted for the publication).

3.1 Removal of dyes monitored using UV-Vis.

To demonstrate the application of the prepared acid catalyst present work studied dyes removal of selected three dye namely MB, MO, and CCA.The photodegradation/adsorption without catalyst and starting material catalyst components such as Fe_3O_4, Fe_3O_4@C, and Fe_3O_4@C-SO_3H screened, respectively. The preliminary study revealed that without a catalyst there was no dye degradation/adsorption was noticed; the optimized Fe_3O_4 (10 mg) showed a limited amount of dye degradation, and with the Fe_3O_4@C (10 mg), moderate dye degradation/adsorption was observed, but in the case of surface modification evidenced for the highest dye degradation/adsorption (Figs. S1-S3), respectively. After completion of the experiment, the dye solution was collected by using syringe filter, and subjected to the ESI-MS. The mass spectra analysis revealed that only methylene blue peak appeared in the spectrum, and no other fragmentation peaks noticed. This directly revealed adsorption of the dye take place on the surface of the modified catalyst, so that, we studied adsorption isotherm kinetics. The systematic studies performed in the presence of Fe_3O_4 under sun light exposure and monitored by UV-Vis absorption is tabulated in Table 2. Photodegradation of an aqueous solution of MB was carried out spectrophotometrically at λ 664 nm using 10 mg of the catalyst (Fe_3O_4@C@SO_3H) added to a solution, and exposed to sunlight, drawn experimental test solution, filtered of catalysts after every 30 min, and collected UV-Vis absorbance (Fig. 2).
Moreover, to change the rate of the degradation in another method, MW irradiation method also performed for MB dye in the presence of catalyst (10 mg). Briefly, MB dye solution was taken in an RB flask, and exposed to MWI for 14 min at the power of 480 W, and each 2 min interval was taken sample for UV-Vis absorption collection, and combined interval time up to 14 min is shown in the Fig. 3.

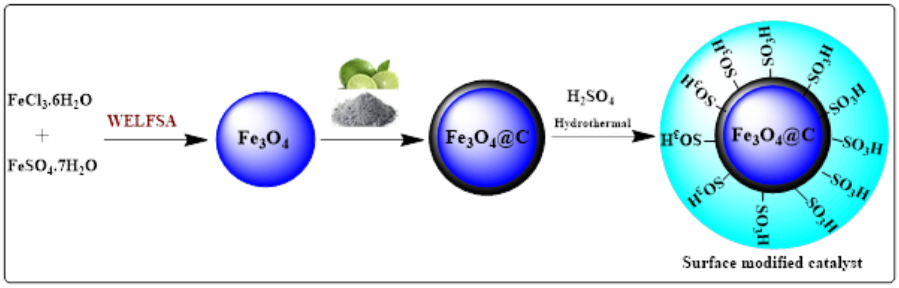

Figure 1. Pictorial representation of Fe_3O_4@C-SO_3H preparation.

Table 2. Kinetic values for MB adsorption.

Catalyst	I order	II order	Intra particle size (IP)
Fe_3O_4	$q_e(m_g\ g^{-1})$=0.3 $k_1\ (min^{-1}) \times 10^{-3}$=11.2 R^2 = -0.280	$q_e(m_g\ g^{-1})$=58.82 $K_2\ (min^{-1}) \times 10^{-3}$=0.017 R^2 =0.9996	C (mg/g) =3.1 k_{id} (g mg^{-1} min^{-1}/2)=1.3 R^2 =0.8
Fe_3O_4 @C	$q_e(m_g\ g^{-1})$=0.8 $k_1\ (min^{-1}) \times 10^{-3}$=13.5 R^2 = -0.257	$q_e(m_g\ g^{-1})$=58.8 $K_2\ (min^{-1}) \times 10^{-3}$=0.014 R^2 =0.994	C (mg/g) =7.3 k_{id} (g mg^{-1} min^{-1}/2)=0.9 R^2 =0.84
Fe_3O_4 @C-SO_3H	$q_e(m_g\ g^{-1})$=1.1 $k_1\ (min^{-1}) \times 10^{-3}$=16.4 R^2 =0.730	$q_e(m_g\ g^{-1})$=57.80 $K_2\ (min^{-1}) \times 10^{-3}$=0.017 R^2 =0.994	C (mg/g) =9.6 k_{id} (g mg^{-1} min^{-1}/2)=1.1 R^2 =0.84

Further to check the catalytic activity of prepared solid acid employed another dye MO without a catalyst is performed under sunlight exposure. The progression of the dye degradation was monitored using UV-Vis at 464 nm withdrawing 1mL of the test solution after each 30 min interval of time (Fig. S4). Then the degradation experiment directly taken MO dyes in the presence of Fe_3O_4@C-SO_3H each 30 min interval time (Fig. S5). Finally, the third CCA dye was taken for the comparative photodegradation studies, in the presence of a catalyst and reaction was monitored in every 30 min interval at λ_{max} 550 nm. (Fig. S6). This study revealed that ,the faster rate of the dye adsorption noticed under MWI is due to heating and absorption of radiation by the reaction medium activate catalysts. Further dye CCA and MO sample also performed under MWI for up to 12 min exposure to MWI, and reaction was monitored by UV–Vis absorption maximum of CCA at 550 nm (Figs. S7 and S8).

3.2 Reduction of 4-nitrophenol

The reduction catalytic activity of the prepared Fe_3O_4@C-SO_3H was performed against 4-nitrophenol in the presence of hydride source $NaBH_4$ at rt using a UV–Vis spectrophotometer. The electrochemical potential of 4-NP (E_0 4NP/4AP) = -0.76 V and that of $NABH_4$ (E_0 H_3BO_3/BH_4^-) = -1.33 V the reduction process is thermodynamically possible but kinetically not favourable because of the mutual repulsion of the negative ions such as nitrophenol and BH_4^-. Therefore, the reaction required catalyst [66, 67]. Fig. 4a shows the UV-Vis absorbance spectra of 4-NP alone and 4-NP with $NaBH_4$ solutions. The absorption peaks at 360 nm and 420 nm correspond to the aqueous solution of 4-NP, which appeared due to n $\rightarrow \pi^*$ and $\pi \rightarrow \pi^*$ transitions [68]. The 4-NP solution is light yellow in colour and it changes to greenish yellow upon adding $NaBH_4$. The change in colour shifts the position of the absorption peak from 319 nm to 400 nm (Fig. 4b). Upon the $NaBH_4$ addition to the 4-NP solution absence of catalysts shows no reduction of the 4-NP observed. In contrast addition of Fe_3O_4@C-SO_3H NPs decreases the intensity at λ_{max} 360 nm. At the same time, a new absorption peak at 400 nm emerged, which corresponds to 4-AP (Scheme 1). To facilitate 4-NP reduction reaction with $NaBH_4$ in the presence of Fe_3O_4@C-SO_3H NPs. Firstly, both 4-NP and $NaBH_4$ were adsorbed on the surface of Fe_3O_4@C-SO_3H NPs, where the electron transfer takes place. This is the redox reaction, where 4-NP accepts the electron, and $NaBH_4$ donates it [68]. To study the effect of $NaBH_4$ on 4-NP reduction, experiments were performed by varying $NaBH_4$ (50mM) volume from 100 μL to 300 μL using 2 mL of 4-NP (0.15mM) and 1 mg of Fe_3O_4@C-SO_3H (Fig. 4c). It was observed that as the volume of $NaBH_4$ increases from 100 μL to 300 μL, the percentage of 4-NP to 4-AP conversion also increases with a marginal difference from 93% to 96%, respectively, in about 10 min.

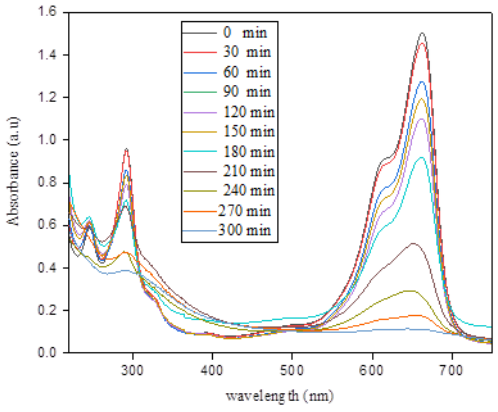

Figure 2. UV-Vis Profile for MB in the presence of a catalyst.

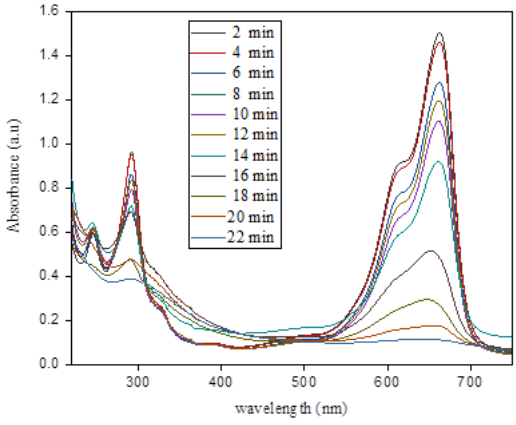

Figure 3. UV-Vis Absorption spectra of MB under MWI.

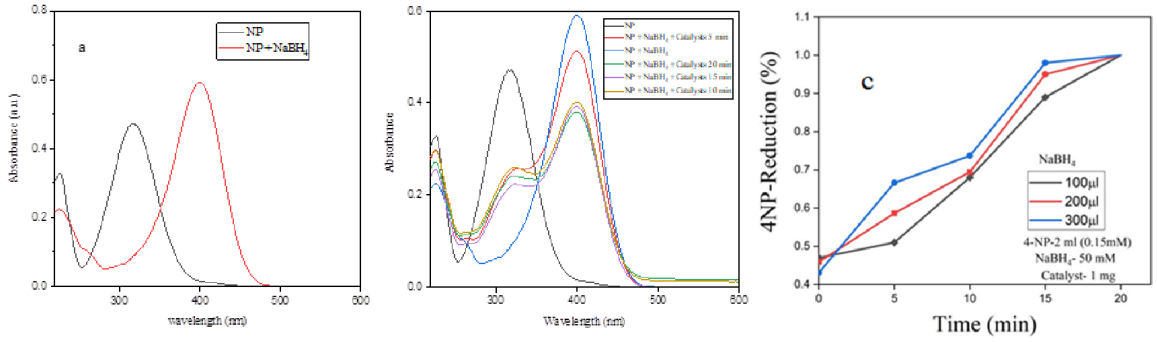

Figure 4. a) UV-Vis spectra of solutions, 4-NP and 4-NP in NaBH4 without catalysts (Reaction condition: 4-NP=2 mL (0.15 mM), $NaBH_4$= 100 μL (50 mM)). b) Time-dependent UV-Vis spectra of 4-NP reduction in NaBH4 with catalysts (Reaction conditions: 4-NP= 2 mL (0.15 mM), $NaBH_4$= 100 μL (50 mM), catalyst=1 mg). c) Effect of volume of $NaBH_4$ on the reduction of 4-NP in Fe_3O_4@C-SO_3H NPs using $NaBH_4$.

3.3 Reduction of methylene blue

The photocatalytic activity of the prepared catalysts has been assessed against MB reduction by $NaBH_4$ at rt using UV–Vis. Fig. 5 shows the UV-Vis spectrum of MB reduction using Fe_3O_4@C-SO_3H in the presence of $NaBH_4$. Here, the absorption band for MB was obtained at 665 nm and 290 nm due to the transition of n $\rightarrow \pi^*$ and $\pi \rightarrow \pi^*$ transition [68]. The addition of $NaBH_4$ into the MB dye does not alter the intensity of the absorption peak at 667 nm. From these observations, it was corroborated that $NaBH_4$ alone does not reduce MB. This was owing to the high reduction potential difference between MB and $NaBH_4$ [69]. However, upon addition of catalysts to the solution of MB and $NaBH_4$ a gradual decrease in the intensity at 665 nm was observed (Scheme 2), which directly reflects the reduction of MB dye, and complete reduction takes place in about 6 min (Fig. 5b). Bhosale et al., [70] and Zheng et al., [71] reported a similar observation with Fe_3O_4 and Fe_3O_4@SiO_2 in the presence of $NaBH_4$. As the reduction of MB takes place, the intensity at 660 nm decreases, concurrently, a new peak at 350 nm emerges, and its intensity increases with time owing to the formation of leuco MB [72]. The effect of $NaBH_4$, its concentration, and the catalyst was studied using 2 mL MB (10 ppm) solution, and the progress of the reduction reaction was monitored by UV–Vis. The mixture of MB and 100 μL of $NaBH_4$ (30 mm) without catalysts shows a negligible (13%) reduction of MB dye (Fig. 5a). However, MB in the presence of 2 mg catalysts without $NaBH_4$ shows a 25% of the decrease in the intensity at 665 nm in about 6 min, which corresponds to the adsorption of dye on the catalyst [73]. Furthermore, the MB reduction (2 mL, 10 ppm) was carried out at 100 μL and 200 μL $NaBH_4$ (30 mM) using 1 mg of the catalysts. In the case of 100 μL of $NaBH_4$, in 2 min (Fig. 5a).

3.4 Adsorption and photocatalytic experiments

The MB removal from the aqueous solution by adsorption depends on the amount of adsorbent, pH, and time. The effect of these parameters was studied by using Fe_3O_4@C-SO_3H on MB, MO, and CCA dye. The adsorption of MB on Fe_3O_4@C-SO_3H was carried out at rt in the dark and natural pH 5. About 10 mg of adsorbent was added to 100 mL of 3.12 × 10-2 M MB solution and stirred at about 300 rpm by magnetic stirrer and noted time as initial. After a fixed interval of time, 1 mL of aliquot was taken by the syringe, and filtered to remove catalyst particles. The concentration of the MB was predictable by using UV-Vis of the characteristic absorption peak of MB at 664 nm. Also, the pH of the dye solution was adjusted to the desired value using 0.1 M NaOH or 0.1 M HCl.

The amount of MB adsorbed was calculated from the following equation

$$q = (C_o - C_e)\frac{V}{m} \quad (1)$$

where q is the amount of dye adsorbed/unit weight of Fe_3O_4@C-SO_3H (mg/g)

C_o – initial concentration of MB (mg/L)

C_e – concentration of MB in solution at equilibrium time (mg/L)

V – volume of solution (L)

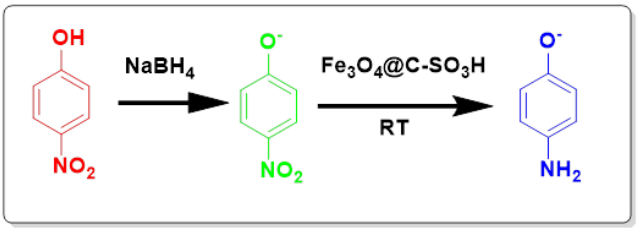

Scheme 1. Catalytic reduction of 4-NP to 4-AP using Fe_3O_4@C-SO_3H.

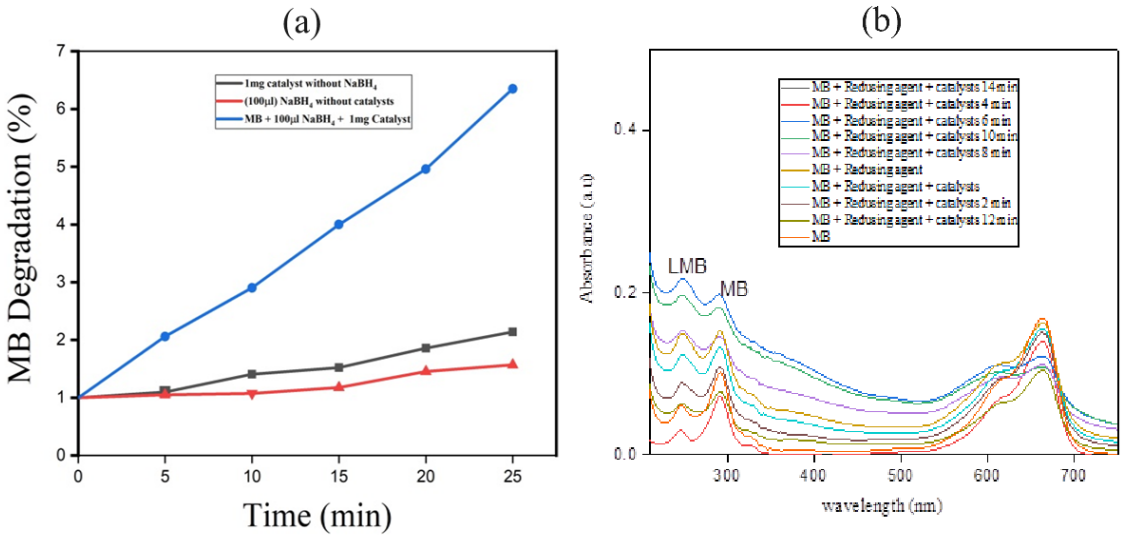

Figure 5. a) Time-dependent UV-Vis spectra of MB reduction in $NaBH_4$ with Fe_3O_4@C-SO_3H (reaction condition: MB = 2 mL (10 ppm), $NaBH_4$= 100 μL (30 mM), catalyst=1 mg). b) Kinetic study of MB reduction using 10 ppm MB solution.

m – weight of Fe_3O_4@C-SO_3H NPs (mg)

$$\text{adsorption}\% = (C_0 - C_i) \times \frac{100}{C_0} \qquad (2)$$

where C_0 and C_i are the initial and final concentrations of the MB solution.

The photocatalytic experiment was carried out in the presence of sunlight. Briefly, taken 100 mL of MB dye (3.12 $\times$ 10^{-2} M) in 10 mg the catalysts (Fe_3O_4@C-SO_3H) was exposed to sunlight up to 3 h. Before going to sunlight exposure, the suspension was stirred in the dark for about 30 min to achieve adsorption/desorption equilibrium. The photodegradition rate for each experiment is calculated by using the following equation.

$$\text{photodegradation rate}\% = (C_0 - C_i) \times \frac{100}{C_0} \qquad (3)$$

In dark condition weak interaction was observed and in presence of the sunlight strong interaction of MB and Fe_3O_4@C-SO_3H was encountered. Thus, sun light was used for the degradation of MB dye. The absorption peaks of MB exhibited at 292 nm and 664 nm in UV-Vis, respectively. The peak in UV region is because of absorption of the π-π^* transition of the aromatic ring, while peak in visible region is due to absorption of n-π^* transition with -N=N- group present in the MB (Fig. 5b).

The degradation of MB is more efficient in the presence of functionalized catalyst Fe_3O_4@C-SO_3H (95.98%) than that of iron oxide alone (34.46%) and Fe_3O_4@C gave 67.56% adsorption shown at absorption maximum 664 nm (Fig. 6). These studies revealed that, the prepared surface functionalized iron oxide had dye adsorption properties, and it served as a hazardous organic dye decolourization.

3.5 Adsorption kinetics

3.5.1 Effect of contact time

The effect of contact time for the removal of MB dye was presented in Fig. 7. The percentage adsorption of MB on Fe_3O_4@C-SO_3H NPs in dark and light condition performed using 100 mL of 2 ppm MB dye solution. In the dark, the adsorption rate found to be slow, and about 40.56% MB is

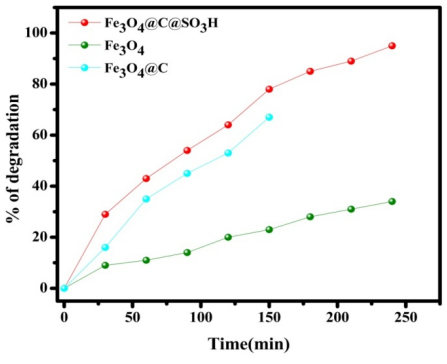

Figure 6. Percentage photocatalytic degradation of MB v/s time.

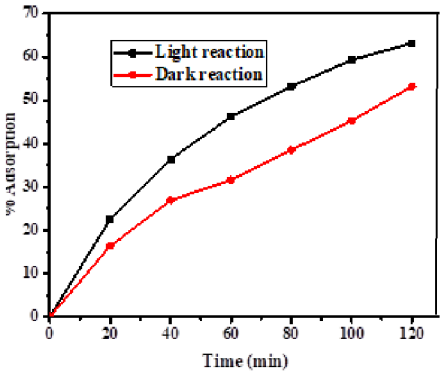

Figure 7. Percentage adsorption of MB in dark and light reaction condition.

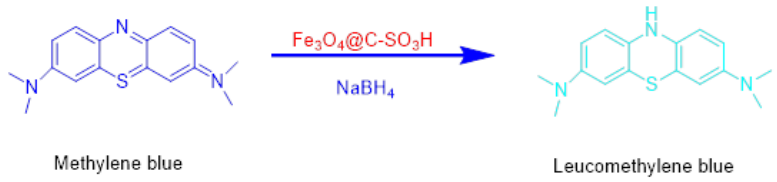

Scheme 2. Catalytic reduction of MB to LMB.

removed, while in the presence of light reaction condition gave 95.98%. There is a fast change in the rate of adsorption because initially, all the adsorbent sites are vacant, and solute concentration gradient is very high. After some time, there is a decreased number of vacant sites of adsorbent and dye concentration, which can cause the low rate of adsorption. The decreased adsorption indicates the possible monolayer formation of the MB on the adsorbent surface.

3.5.2 Effect of pH

As shown in Fig. 8, the sharp increase amount of MB adsorbed noticed pH 1 to 3. At pH 5, SO_3H group would be deprotonated, exposing more negative charges, and other side more cationic MB present involved strong electrostatic interaction. Above pH 9, the amount of MB adsorbed remained constant. The lowest amount of MB adsorbed at pH 1– 3, was due to the competition of cationic MB with H^+ ions in an acidic solution.

Adsorption kinetic for the MB onto the catalysts surface was explored by applying pseudo-first-order and pseudo-second-order models. The models are expressed by equations 4 and 5, respectively.

$$\log(q_e - q_t) = \log q_e - \frac{k_1}{2.303}t \tag{4}$$

$$\frac{t}{q_t} = \frac{1}{h} + \frac{1}{q_e} \tag{5}$$

where q_t (mg/g) and q_e (mg/g) are the amount of MB adsorbed at time t (min) in equilibrium, respectively.

K_1 (min^{-1}) is the pseudo-first-order rate constant, h [mg/(g.min)] is the initial adsorption rate in the pseudo-second-order equation and can be calculated as $h = K_2 q_e^2$. $K_2 g$ (mg.min) is the pseudo-second-order rate constant. The

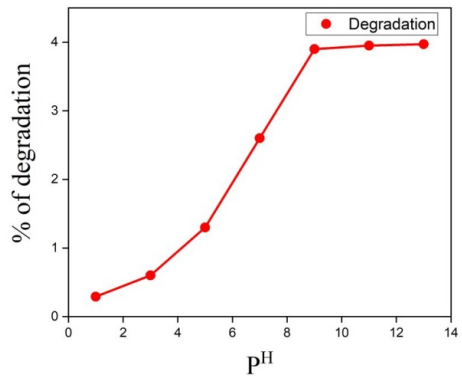

Figure 8. Effect of pH on MB adsorption.

Pseudo second-order plot has higher linearity with R^2 close to unity compared to the pseudo first-order model, the best fit for pseudo second order kinetic resulted and shown in (Table. 2).

Pseudo 1^{st} order kinetics and pseudo 2^{nd} order kinetics are presented in Figs. 9 and 10.

3.5.3 Intraparticle diffusion

The intra diffusion particle of MB on Fe_3O_4, Fe_3O_4@C, Fe_3O_4@C-SO_3H NPs in light & dark condition. Here the intra particle diffusion is immatter of the quantity of the catalyst by increase in the quantity the rate constant is found to be same and it is mentioned in the supporting information as Fig. S12.

The calculated amount of MB adsorbed ($q_{e,calc}$) of pseudo-second-order model showed values close to the experimental values ($q_{e,exp}$). Therefore, the adsorption process is best fitted to the pseudo-second-order model, and the complexation reaction could be the rate-determining step.

3.6 Adsorption isotherm

3.6.1 Langmuir isotherm

To study the adsorption capacity of the Fe_3O_4@C-SO_3H NPs on MB, Langmuir isotherm was monitored in the presence of dark and light reaction condition at rt as shown in Fig. 11. This model was a theoretical concept and only applicable to monolayer formation on the outer surface of the adsorbent considered. Thus, the Langmuir model is equilibrium distribution of metal ion between solid and liquid phase and it is expressed as,

$$q_e = q_m K_L . \frac{c_e}{1} + K_L C_e \tag{6}$$

q_m and K_L are the constants of Langmuir equation

The linear form of Langmuir isotherm

$$\frac{1}{q_e} = \frac{1}{q_m} + \frac{1}{q_m} K_L C_e \tag{7}$$

where C_e= is the equilibrium concentration (mg/L),

q_e=is the amount of MB adsorbed (mg/g),

q_m= is the extreme quantity of adsorption (mg/g),

K_L= is sorption equilibrium constant (L/mg).

The values of q_m and K_L were calculated from the slope and intercepted Langmuir plot of $1/q$ eV/s $1/C_e$ (Table 3).

3.6.2 Freundlich isotherm

Freundlich isotherm was performed in the presence of dark and light reaction condition at rt as shown in Fig. 12. Freundlich isotherm is valid for the heterogeneous surface of an adsorbent for both monolayer and multilayer adsorption.

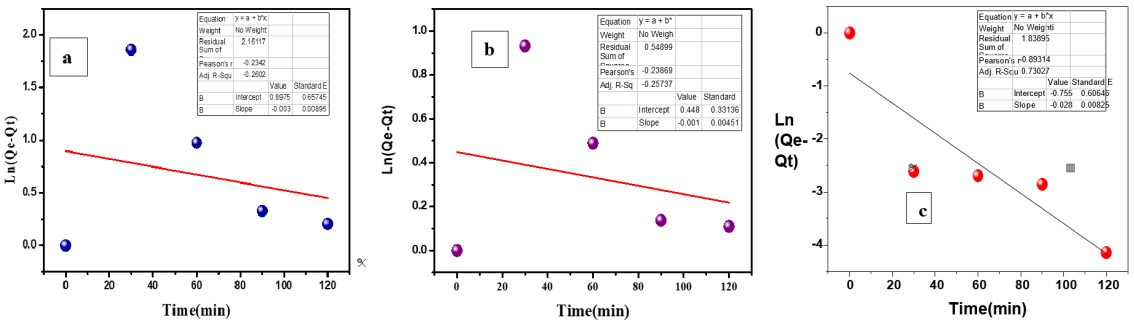

Figure 9. Pseudo first order kinetics of MB on: a) Fe_3O_4, b) Fe_3O_4@C, and c) Fe_3O_4@C-SO_3H NPs in light & dark condition.

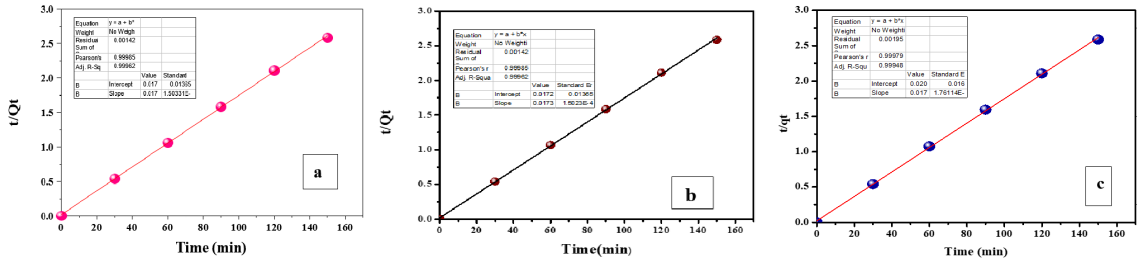

Figure 10. Pseudo 2^{nd} order kinetics of MB on: a) Fe_3O_4, b) Fe_3O_4@C, and c) Fe_3O_4@C-SO_3H NPs.

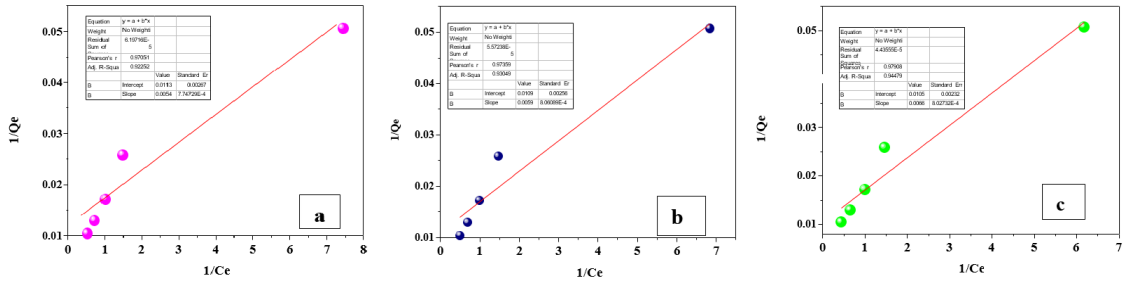

Figure 11. Langmuir isotherm of MB on: a) Fe_3O_4, b) Fe_3O_4@C, and c) Fe_3O_4@C-SO_3H NPs in light & dark condition.

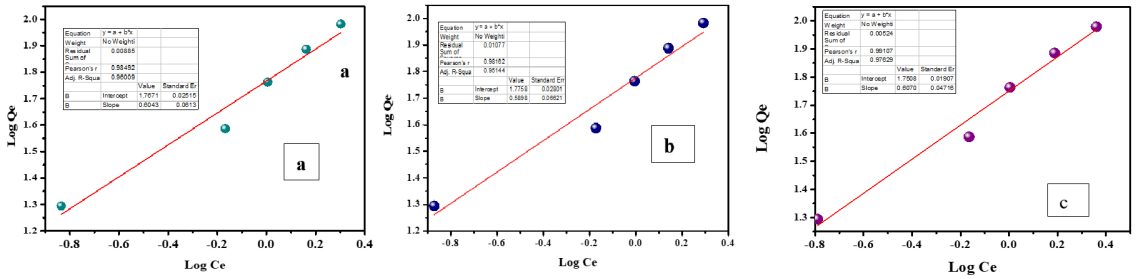

Figure 12. Freundlich isotherm of MB on: a) Fe_3O_4, b) Fe_3O_4@C, and c) Fe_3O_4@C-SO_3H NPs in light & dark condition.

The Freundlich isotherm equation is expressed as,

$$q_e = K_F C_e^{1/n} \tag{8}$$

where K_F = Freundlich isotherm constant (mg/g), n=adsorption intensity, C_e=the equilibrium concentration of adsorbate (mg/L), q_e = the amount of metal adsorbed per gram of the adsorbent at equilibrium, (mg/g). The linear form of Freundlich isotherm is

$$\ln q_e = \ln K + \frac{1}{n} \ln C_e \tag{9}$$

The values of n and K_F were calculated from the plot of $\ln q_e$ v/s $\ln C_e$ (Table 3).

The adsorption mechanism on the surface modified catalyst is depicted in the supporting data as Fig. S9. This mechanism well revealed that the formation of the electro-

Table 3. Isotherm model fitting results for MB isotherm adsorption on catalyst.

Catalyst	Freundlich	Langmuir
Fe_3O_4	K_F (mg/g)/(mg/L)n = 59.67 1/n = 0.58 R^2 = 0.95	q_m (mg/g) =88.49 K_L (L/m_g)=2.09 R^2 = 0.922
Fe_3O_4 @C	K_F (mg/g)/ (mg/L) n =56.33 1/n = 0.60 R^2 = 0.976	q_m (mg/g) =95.238 K_L (L/m_g) =1.590 R^2 =0.944
Fe_3O_4 @C-SO_3H	K_F (mg/g)/ (mg/L) n =58.49 1/n = 0.604 R^2 = 0.9600	q_m (mg/g) =91.743 K_L (L/m_g) =1.8474 R^2 = 0.9304

Table 4. Summary of this study.

Catalyst	Source	Dye	Time	% of Degradation
Without catalyst	Sunlight	Methylene Blue	300 min.	3.5
Fe_3O_4	Sunlight	Methylene Blue	240 min	34.46
Fe_3O_4@C	Sunlight	Methylene Blue	240 min	67.56
Fe_3O_4@C-SO_3H	Sunlight	Methylene Blue	240 min	95.98
Without catalyst	Sunlight	Methyl Orange	240 min.	5.4
Fe_3O_4@C-SO_3H	Sunlight	Methyl Orange	240 min.	82.55
Fe_3O_4@C-SO_3H	Sunlight	Calcancarboxylic acid	240 min.	83.7
Fe_3O_4@C-SO_3H	Microwave	Methylene Blue	2 min.	92.03%
Fe_3O_4@C-SO_3H	Microwave	Calcancarboxylic acid	4 min.	77.15%
Fe_3O_4@C-SO_3H	Microwave	Methyl Orange	4 min.	78.17%

static interaction, pi to pi-interaction, and hydrogen bonding formation leads to hold the dye on the catalyst surface [74].

3.7 Adsorbent product was characterization by LC-MS

After sunlight exposure, the reaction sample was concentrated to reduce the volume, and resulted sample subjected to liquid chromatography–mass spectrometry (HR-MS). The reaction sample of the MB dye was analysed, and the data shown in Fig. S13. The prominent peak at 330.9 Da, which is the molecular weight of the MB, was obtained after 4 h exposure to sunlight of the MB dye in the presence of the catalysts. This revealed the catalysts surface is active and in negative charge, capable to adsorb positively charged dye like MB faster instead of the degradation of the dye. The degradation profiles are appended in the supporting data.

4. Conclusion

In the present work, we demonstrated our previously prepared surface functionalised iron oxide MNPs (Fe_3O_4@C-SO_3H) employed to toxic organic dyes removal studies. The comparative study of MB, MO, and CCA dyes in both sunlight and MWI was performed, and summarized results were presented in Table 4. Herein noticed efficient dye adsorption on the surface of the modified catalyst with the primary and secondary electronic interactions assumed, and well mentioned in the mechanism. Further required adsorption phenomenon, equilibrium isotherm, and thermodynamics kinetic study of the MB was established.

Acknowledgement
The authors are thankful to the SERB-SURE, GOI (SUR/2022/002631) and RCUB (RCU-IDR-2022-23) for the financial support to Dr. KK.

Supplementary information
Catalyst characterization and UV-Vis Profiles are available in supplementary.

Authors Contributions
Authors were equally contributed in acquisition and analysing the data as well as preparing the paper.

Availability of Data and Materials
Data is available on request from the corresponding author, upon reasonable request.

Conflict of Interests
The authors declare that they have no known competing financial interests or personal relationships that could have appeared to influence the work reported in this paper.

References

[1] X. Xiong, H. Zhang, R. Wang, Z. Tang, and M. Yang. *ACS EST Water*, **3**(2021):404–414. DOI: https://doi.org/10.1021/acsestwater.4c00169.

[2] S. Dutta, B. Gupta, S. K. Srivastava, and A. K. Gupta. *Mater. Adv*, **2**(2021):4497–4531. DOI: https://doi.org/10.1039/D1MA00354B.

[3] I. M. Banat, P. Nigam, D. Singh, and R. Marchant. *Bioresour. Technol*, **58**(1996):217–227. DOI: https://doi.org/10.1016/S0960-8524 (96)00113-7.

[4] L. Y. Zhanga, W. Zhanga, Z. Zhoua, C. M. Li, and J. Colloid. *Interface. Sci*, **476**(2016):200–205. DOI: https://doi.org/10.1016/j.jcis.2016.05.025.

[5] H. Langhals. *Angew. Chem. Int. Ed*, **43**(2004):5291–5292. DOI: https://doi.org/10.1002/anie.200485174.

[6] S. Karishma, P. R. Yaashikaa, P. Senthil Kumar, R. Kamalesh, A. Saravanan, and G. Rangasamy. *Environ. Sci. Adv*, **2**(2023):1488–1504. DOI: https://doi.org/10.1039/D3VA00194F.

[7] I. K. Konstantinou and T. A. Albanis. . *Appl. Catal B*, **49**(2004):1–14. DOI: https://doi.org/10.1016/j.apcatb.2003.11.010.

[8] N. Singh and B. R. Goldsmith. . *ACS Catal*, **10**(2020):3365–3371. DOI: https://doi.org/10.1021/acscatal.9b04167.

[9] A. Bafana, S. S. Devi, and T. Chakrabarti. *Environ. Rev*, **19**(2011):350–371. DOI: https://doi.org/10.1139/a11-018.

[10] M. Afzal, K. Rehman, G. Shabir, R. Tahseen, A. Ijaz, A. J. Hashmat, and H. Brix. . *npj Clean Water*, **2**(2019):3. DOI: https://doi.org/10.1038/s41545-018-0025-7.

[11] K. L. Offenbaume, E. Bertone, and R. A. Stewart. . *Water*, **12**(2020):2591. DOI: https://doi.org/10.3390/w12092591.

[12] T. Yahagi, M. Degawa, Y. Seino, T. Matsushima, M. Nagao, T. Sugimura, and Y. Hashimoto. *Cancer Lett*, **1**(1975):91–96. DOI: https://doi.org/10.1016/S0304-3835.

[13] S. Nam and V. Renganathan. *Chemosphere*, **40**(2000):351–357. DOI: https://doi.org/10.1016/S0045-6535(99)00226-X.

[14] B. J. Singh, A. Chakraborty, R. Sehgal, and J. Environ. . *Manag*, **348**(2023):119230. DOI: https://doi.org/10.1016/j.jenvman.2023.119230.

[15] R. A. Tohamya, S. S. Alia, F. Li, K. M. Okasha, Y. A. G. Mahmoud, T. Elsamahya, H. Jiaoa, Y. Fua, and J. Sun. . *Ecotoxicol. Environ. Safety*, **231**(2022):113160. DOI: https://doi.org/10.1016/j.ecoenv.2021.113160.

[16] M. J. Prival, S. J. Bell, V. D. Mitchell, M. D. Peiperl, and V. L. Vaughan. . *Mutat. Res*, **136**(1984):33–47. DOI: https://doi.org/10.1016/0165-1218(84)90132-0.

[17] L. He, F. Michailidou, H. L. Gahlon, and W. Zeng. . *Chem. Res. Toxicol*, **35**(2022):901–915. DOI: https://doi.org/10.1021/acs.chemrestox.1c00427.

[18] R. A. Tohamy, S. S. Ali, F. Li, K. M. Okasha, Y. A. G. Mahmoud, T. Elsamahy, H. Jiao, Y. Fu, and J. Sun. . *Ecotoxicol. Environ. Safety.*, **231**(2022):113160. DOI: https://doi.org/10.1016/j.ecoenv.2021.113160.

[19] S. Sansuk and S. Srijaranai. . *Environ. Sci. Technol.*, **50**(2016):6477–6484. DOI: https://doi.org/10.1021/acs.est.6b00919.

[20] S. Parlayıcı and E. Pehlivan. . *Int. J. Phytoremediation.*, **23**(2021):26. DOI: https://doi.org/10.1080/15226514.2020.1788502.

[21] L. Wu, X. Liu, G. Lv, R. Zhu, L. Tian, M. Liu, Y. Li, W. Rao, T. Liu, and L. Liao. . *Sci Rep.*, **11**(2021):10640. DOI: https://doi.org/10.1038/s41598-021-90235-1.

[22] E. A. Alabbad. . *Open Chem J*, **7**(2020):16. DOI: https://doi.org/10.2174/1874842202007010016.

[23] B. Tunçsiper. . *J. Clean. Prod*, **228**(2019):1368. DOI: https://doi.org/10.1016/j.jclepro.2019.04.211.

[24] K. S .Bharathi and S. T. Ramesh. . *Appl. Water. Sci.*, **3**(2013):773. DOI: https://doi.org/10.1007/s13201-013-0117-y.

[25] Y. Dai, Q. Sun, W. Wang, L. Lu, M. Liu, J. Li, S. Yang, Y. Sun, K. Zhang, J. Xu, W. Zheng, Z. Hu, Y. Yang, Y. Gao, Y. Chen, X. Zhang, F. Gao, and Y. Zhang. . *Chemosphere*, **211**(2018):235. URL 10.1056/NEJMoa1300955.

[26] M. R. Panuccio Sorgonà, A. M. Rizzo, and G. Cacco. . *J. Environ. Manage*, **90**(2009):364. DOI: https://doi.org/10.1016/j.jenvman.2007.10.005.

[27] X. Huang, N. Y. Gao, and Q. L. Zhang. Thermodynamics and kinetics of cadmium adsorption onto oxidized granular activated carbon. *J. Environ. Sci.*, **19**(2007):1287. DOI: https://doi.org/10.1016/s1001-0742(07)60210-1.

[28] T. J. Bamgbose, S. Adewuyi, O. Bamgbose, and A. A. Adetoye. . *Afr. J. Biotechnol*, **9**(2010):2560. DOI: https://doi.org/1021-9986/15/3/25.

[29] J. Hizal and R. Apak. Modeling of cadmium (II) adsorption on kaolinite-based clays in the absence and presence of humic acid. *Appl. Clay. Sci.*, **32**(2006): 232. DOI: https://doi.org/10.1016/j.clay.2006.02.002.

[30] G. C. Panda, S. K. Das, and A. K. Guha. Biosorption of cadmium and nickel by functionalized husk of Lathyrussativus. *Colloids Surf B*, **62**(2008):173. DOI: https://doi.org/10.1016/j.colsurfb.2007.09.034.

[31] S. J. Peighambardoust, R. Foroutan, S. H. Peighambardoust, H. Khatooni, and B. Ramavandi. . *Chemosphere*, **282**(2021):131088. DOI: https://doi.org/10.3390/ma15196964.

[32] V. K. Gupta and A. Nayak. . *Chem. Eng. J.*, **180**(2012): 81. DOI: https://doi.org/10.1016/j.cej.2011.11.006.

[33] R. Jiang, J. Tian, H. Zheng, J. Qi, S. Sun, and X. Li. *J. Environ .Manage*, **155**(2015):24. DOI: https://doi.org/10.1039/d3ra00723e.

[34] D. M. Patila, K. T. Chandrashekara, J. Manjannaa, and M. B. Sridhara. . *Iranian. Journal of Catalysis*, **13**(2023)(1):47–5. DOI: https://doi.org/10.30495/IJC.2023.1972239.1972.

[35] P. Anitha, A. Ramachandran, R. Sudha, N. Valarmathi, and D. Geetha. . *Indian J Chemical. Techn*, **31**(2024):355–368. DOI: https://doi.org/10.56042/ijct.v31i3.7041.

[36] K. Saeed, I. Khan, T. Gul, and M. Sadiq. . *Appl. Water. Sci*, **7**(2017):3841–8. DOI: https://doi.org/10.1007/s10854-020-03431-6.

[37] M. Valaskova, J. Tokarsky, J. Pavlovsky, T. Prostejovsky, and K. Kocí. . *Materials*, (2019):121880. DOI: https://doi.org/10.1007/s40201-020-00563-z.

[38] Y. Liu, N. Sun, J. Hu, S. Li, and G. Qin. . *R Soc Open Sci*, **5**(2018):172196. DOI: https://doi.org/10.1016/j.addma.2022.102691.

[39] T. Ma, L. Zheng, Y. Zhao, Y. Xu, J. Zhang, and X. Liu. . *ACS Appl. Nano. Mater*, **2**(2019):2347–57. DOI: https://doi.org/10.1021/acsami.0c13070.

[40] D. M. S. N. Dissanayake, M. M. M. G. P. G. Mantilaka, T. C. Palihawadana, G. T. D. Chandrakumara, R. T. D. Silva, H. M. T. G. A. Pitawala, K. M. N. Silva, and G. A. J. Amaratunga. . *RSC Adv*, **9**(2019):21249–212257. DOI: https://doi.org/10.1039/C9RA03756J.

[41] Y. Ge, M. Hoque, and Q. Qu. . *Electrochem. Energy. Technol*, **5**(2019):1–6. DOI: https://doi.org/10.1201/9781003145585-5.

[42] J. Kim, J. Hwang, Y. Sun, and J. Hassoun. *Sustain Energy Fuels*, **3**(2019):2675–87. DOI: https://doi.org/10.1039/C8SE00442K.

[43] V. Harnchana, S. Chaiyachad, S. Pimanpang, C. Saiyasombat, P. Srepusharawoot, and V. Amornkitbamrung. . *Sci Rep*, **9**(2019). DOI: https://doi.org/10.1007/s40201-020-00563-z.

[44] G. Darmograi, B. Prelot, A. Geneste, G. Martin-Gassin, F. Salles, and J. Zajac. . *J. Phys. Chem. C*, **120**(2016):10410–10418. DOI: https://doi.org/10.1021/acs.jpcc.6b01888.

[45] Z. Li, B. Yang, S. Zhang, B. Wang, and B. Xue. . *J. Colloid Interface Sci*, **12**(2014):10202–10210. DOI: https://doi.org/10.1039/C4TA01028K.

[46] M. Del Arco, S. Gutierrez, C. Martin, and C. V. Rives. . *Phys. Chem*, **3**(2001):119–126. DOI: https://doi.org/10.3390/chemengineering6040060.

[47] N. B. H. Abdelkader, A. Bentouami, Z. Derriche, N. Bettahar, and L. C. De Menorval. . *J. Chem. Eng*, **169**(2011):231–238. DOI: https://doi.org/10.1039%2Fd0ra04898d.

[48] J. Bai, Y. Liu, X. Yin, H. Duan, and J. Ma. . *Appl. Surf. Sci*, **416**(2017):45–50. DOI: https://doi.org/10.1039/C7RA07417D.

[49] F. T. Zhang, X. Long, D. W. Zhang, Y. L. Sun, Y. L. Zhou, Y. R. Ma, L. M. Qi, and X. X. Zhang. . *Sens. Actuators B Chem*, **192**(2014):150–156. DOI: https://doi.org/10.1016/j.snb.2013.10.097.

[50] M. Luaibi, M. A. Atiya, A. K. Hassan, and Z. A. Mahmoud. . *Karbala Int. J. Mod. Sci*, **8**(2022):9e28. DOI: https://doi.org/10.33640/2405-609X.3217.

[51] Y. Gao, W. Zhu, J. Li, W. Liu, X. Li, J. Zhang, and T. Huang. . *J. Environ*, **121**(2022):148–158. DOI: https://doi.org/10.1016/j.jes.2021.09.024.

[52] N. Semwal, D. Mahar, M. Chatti, A. Dandapat, and M. C. Arya. . *Heliyon*, **9**(2023):e22027. DOI: https://doi.org/10.1016/j.Heliyon.2023.e22027.

[53] D. G. Strawn. . *Soil Syst*, **5**(2021):13. DOI: https://doi.org/10.3390/soilsystems5010013.

[54] O. P. Murphy, M. Vashishtha, P. Palanisamy, and K. V. Kumar. . *ACS. Omega*, **8**(2023):17407–17430. DOI: https://doi.org/10.1021/acsomega.2c08155.

[55] Y. Wang, Z. Wang, Y. Rui, and M. Li. . *Biosens. Bio. electron*, **64**(2015):57–62. DOI: https://doi.org/10.1016/j.bios.2014.08.054.

[56] A. Safavi and S. Momeni. . *Biosens. Bio electron*, **201**(2012):125–131. DOI: https://doi.org/10.1016/j.molliq.2016.08.058.

[57] M. Zhu and G. Diao. . *J. Phys. Chem. C*, **115**(2011):18923–18934. DOI: https://doi.org/10.1021/jp052678c.

[58] H. Veisi, S. Razeghi, P. Mohammadi, and S. Hemmati. . *Mater. Sci. Eng. C*, **97**(2019):624–631. DOI: https://doi.org/10.1039/C9RA08809A.

[59] S. Rahim Pouran, A. Bayrami, A. R. A. Aziz, W. M. A. W. Daud, and M. S. Shafeeyan. . *J. Mol. Liq*, **222**(2016):1076–1084. DOI: https://doi.org/10.48175/594.

[60] N. Jaafarzadeh, A. Takdastan, S. Jorfi, F. Ghanbari, M. Ahmadi, and G. Barzegar. . *J. Mol. Liq*, **256**(2018):462–470. DOI: https://doi.org/10.1016/j.molliq.2018.02.047.

[61] J. Saffari, N. Mir, D. Ghanbari, K. Khandan-Barani, A. Hassanabadi, and M. R. Hosseini-Tabatabaei. . *J. Mater. Sci. Mater. Electron*, **26**(2015): 9591–9599. DOI: https://doi.org/10.1088/1755-1315/276/1/012059.

[62] G. C. Silva, V. S. T. Ciminelli, A. M. Ferreira, N. C. Pissolati, P. R. P. Paiva, and J. L. Lopez. . *Mater. Res. Bull*, **49**(2014):544–551. DOI: https://doi.org/10.1039/D3NA00754E.

[63] K. Pakzad, H. Alinezhad, and M. Nasrollahzadeh. . *Ceram. Int*, **45**(2019):17173–17182. DOI: https://doi.org/10.1016/j.btre.2020.e00518.

[64] M. S. Najafinejad, P. Mohammadi, M. Mehdi Afsahi, and H. Sheibani. . *Mater. Sci. Eng. C*, **98**(2019):19–29. DOI: https://doi.org/10.1016/j.molliq.2018.04.052.

[65] L. Gnanasekaran, R. Hemamalini, S. Rajendran, J. Qin, M. L. Yola, N. Atar, and F. Gracia. . *J. Mol.Liq*, **287**(2019):110967–68. DOI: https://doi.org/10.1016/j.molliq.2019.110967.

[66] A. S. Hashimi, M. A. N. Mohd Nohan, S. X. Chin, S. Zakaria, and C. H. Chia. . *Nanomaterials*, **9**(2019): 936. DOI: https://doi.org/10.3390/nano9070936.

[67] V. Lomonosov, J. Asselin, and E. Ringe. . *React. Chem. Eng*, **26**(2022):1728–1741. DOI: https://doi.org/10.1039/d2re00044j.

[68] L. Ai, H. Yue, and J. Jiang. . *J. Mater. Chem*, **22**(2012):23447–23453. DOI: https://doi.org/10.1039/C2JM35616C.

[69] R. Vijayan, S. Joseph, and B. Mathew. . *Bio. Nano. Sci*, **8**(2018):105–117. DOI: https://doi.org/10.1080/24701556.2019.1661439.

[70] M. A. Bhosale, K. D. Bhatte, and B. M. Bhanage. . *Chem.Select*, **235**(2013):516–519. DOI: https://doi.org/10.1016/j.powtec.2012.11.006.

[71] M. Gohain, K. Laskar, H. Phukon, U. Bora, D. Kalita, and D. Deka. . *Waste. Manag. Res*, **102**(2020):212–21. DOI: https://doi.org/10.1002/bbb.2252.

[72] J. S. Ghomi and Z. Samadi. . *RSC*, **11**(2021):35988–35993. DOI: https://doi.org/10.1039/D1RA05848G.

[73] S. Goswami, K. Ghosh, and R. Mukherjee. . *Tetrahedron*, **57**(2023):4987–4993. DOI: https://doi.org/10.1016/S0040-4020(01)00428-8.

[74] B. Y. Mekonnen, G. Y. Abate, S. D. Mekonnen, and A. G. Gebeyehu. . *Indian. J. Chem*, **30**(2023):94–102. DOI: https://doi.org/10.56042/ijct.v30i1.62337.